DOI: 10.1002/cctc.201000273

Aberration-corrected Analytical Microscopy Characterization of Double-Supported $WO_3/TiO_2/SiO_2$ Solid Acid Catalysts

Wu Zhou,[a] Kevin F. Doura,[b] Masashi Watanabe,[a] Andrew A. Herzing,[c] Eiji Okunishi,[d] Elizabeth I. Ross-Medgaarden,[b] Israel E. Wachs,[b] and Christopher J. Kiely*[a]

Double-supported metal oxide catalysts, in which an oxide support material with a high surface area is modified by the presence of a second metal oxide surface species added to control the distribution and activity of a third active oxide component, represent a significant challenge in terms of structural characterization. In this study the various components in a double-supported $WO_3/TiO_2/SiO_2$ catalyst system are effectively visualized by using complementary high-angle annular dark field (HAADF) and bright field (BF) imaging within an aberration-corrected scanning transmission electron microscope (STEM). Furthermore, if combined with chemical analysis by electron energy-loss spectroscopy (EELS) and X-ray energy-dispersive spectroscopy (XEDS) within the same STEM instrument, it is possible to map out the relative spatial distribution of all the metal oxide components within the $WO_3/TiO_2/SiO_2$ catalysts. By comparing the structures of a systematic set of $WO_3/TiO_2/SiO_2$ samples that display high, intermediate and low activity for the methanol dehydration reaction, new insight is provided into the structure-performance relationships that exist in this double supported catalyst system.

Introduction

The concept of rational design and the controlled synthesis of atomically engineered catalyst nanostructures, with the goal of tailoring the catalytic performance, is currently receiving considerable attention from both academia and industry.[1–8] Such deliberate material design protocols and novel synthesis methods often lead to complex catalyst nanostructures, which present significant structural characterization challenges. It is essential that the challenges are overcome in order to establish a detailed understanding of the catalyst nanostructure and to elucidate any structure–performance relationships.[5,9]

One approach to control the nanostructure and properties of catalysts is to modify the surface of the support materials. For example, it has been shown that if a SiO_2 surface is covered by titania islands prior to depositing Au catalyst particles, then the thermal stability of the supported Au nanoparticles is significantly improved as compared to unmodified supported Au/SiO_2 catalysts.[10,11] The Au in this case was thought to preferentially associate itself with the TiO_2 islands.[10,11] More recently, Ross-Medgaarden et al. reported one of the first systematic studies on a model double-supported metal oxide catalyst system (i.e., $WO_3/TiO_2/SiO_2$),[12] in which the WO_x active species were dispersed on a titania-modified SiO_2 support. By carefully controlling the lateral dimension of the titania rafts, and thus their electronic structure (as measured by UV/Vis edge energy, E_g), they were able to tune the electron-transfer behavior between the active surface WO_x species and the underlying TiO_2 domains to maximize their catalytic performance. High-resolution transmission electron microscopy (HRTEM) and a variety of in situ optical spectroscopy techniques (Raman, infrared, and UV/Vis) were applied to the structural and chemical characterization of this set of catalysts. From the extensive characterization studies, Ross-Medgaarden et al. proposed that WO_x was molecularly dispersed and preferentially anchored to the TiO_x rafts instead of directly to the amorphous SiO_2 surface, owing to the stronger interaction between the surface WO_x species and the TiO_x. However, they were unable to directly observe the atomic scale surface structure and spatial distribution of these different metal oxide species, owing to the limitations of the characterization techniques employed. Indeed, to the best of our knowledge, no work has been reported on the atomic scale surface structural and compositional analysis of such a complex oxide catalyst system comprised of multiple components (in this case WO_x, TiO_x, and SiO_2). In this paper we extend the previous work of Ross-Medgaarden et al. by presenting a more detailed structural characterization of the $WO_3/TiO_2/SiO_2$ catalyst system.

[a] W. Zhou, Prof. M. Watanabe, Prof. C. J. Kiely
Department of Materials Science & Engineering, Lehigh University
5 E. Packer Ave, Bethlehem, PA 18015 (USA)
Fax: (+1) 610-758-4244
E-mail: chk5@lehigh.edu

[b] K. F. Doura, Dr. E. I. Ross-Medgaarden, Prof. I. E. Wachs
Department of Chemical Engineering, Lehigh University
Bethlehem, PA 18015 (USA)

[c] Dr. A. A. Herzing
National Institute of Standards and Technology
Surface and Microanalysis Science Division
Gaithersburg, MD 20899 (USA)

[d] Dr. E. Okunishi
Electron Optics Division, JEOL Ltd.
Tokyo, 196-8558 (Japan)

Supporting information for this article is available on the WWW under http://dx.doi.org/10.1002/cctc.201000273.

Table 1. Dominant surface TiO_x structure and catalytic activity of a sub-set of the double-supported $WO_3/TiO_2/SiO_2$ catalysts. Data adapted from Reference [12].

Sample identification	WO_3 loading [wt%]	TiO_2 loading[a] [wt%]	Dominant surface TiO_x structure[a]	Activity[b] (normalized)
1	5	30	3–5 nm TiO_2 (anatase) nanoparticles	1
2	5	5	isolated and polymeric TiO_x structure	11.2
3	5	12	polymeric TiO_x structure	6.1

[a] Determined from previous UV/Vis spectroscopy and HRTEM experiments; [b] activity measured as turnover frequency (TOF) for steady-state methanol dehydration to dimethyl ether at 573 K. The activities are normalized to a TOF value of 3.3×10^{-3} s^{-1}.

Scanning transmission electron microscopy (STEM) has proven to be one of the most powerful techniques for the structural characterization of heterogeneous catalysts.[13,14] In particular, aberration-corrected high-angle annular dark field (HAADF) imaging, which can provide atomic number (*Z*) contrast information with atomic-scale spatial resolution and single-atom sensitivity,[15,16] has been successfully employed to image the structure of both the supported metal[13,15,17,18] and the supported metal oxide[19,20] catalysts. However, for HAADF *Z*-contrast imaging to be effective, there needs to be a significant difference in atomic number between the various atomic species. For TiO_2/SiO_2 materials, the TiO_2 rafts cannot be easily identified from the SiO_2 support by using HAADF imaging because of the relatively small *Z* difference between Ti ($Z=22$) and Si ($Z=14$, As shown in Figure S1 A in the Supporting Information,). Alternatively, bright field (BF) STEM imaging, or optically equivalent HRTEM imaging,[21] can provide phase contrast information with atomic resolution. The crystalline TiO_2 particles can be well resolved on the amorphous SiO_2 surface by using HRTEM (As shown in Figure S1 B in the Supporting Information). However, imaging a two-dimensional monolayer surface structure with BF-STEM (or HRTEM) gives an extremely low image contrast and interpretation, for which it is difficult to analyze the catalytically active structures in many interesting systems. For example, in the case of the double-supported $WO_3/TiO_2/SiO_2$ catalyst (Figure S1 B), previous optical spectroscopy results[12] have suggested that the WO_x species preferentially adopt a sub-monolayer structure on TiO_2 rafts. Information regarding the structure and spatial distribution of the active WO_x surface species, however, cannot be readily obtained from phase contrast images, as they lack long-range periodicity and are difficult to distinguish relative to the underlying background material. A major advantage of a STEM instrument is that a variety of different signals can be collected simultaneously through different detectors. Here we show that using complementary HAADF and BF-STEM imaging in an aberration-corrected electron microscope, in combination with electron energy loss, and X-ray energy-dispersive spectroscopies (EELS and XEDS, respectively), can provide the atomic-scale information necessary to further refine our understanding of the relationship between structure and activity in this double-supported $WO_3/TiO_2/SiO_2$ catalyst system.

Results and Discussion

A subset of the double-supported $WO_3/TiO_2/SiO_2$ catalysts described in the paper by Ross-Medgaarden[12] was chosen for this study. The catalyst composition, dominant surface TiO_x structure, and the acidic catalytic activity of these three samples are listed in Table 1. All samples contained the same WO_3 loading (5 wt%), whereas the TiO_2 loading in the three samples was varied over a considerable range (5–30 wt%). As the catalytic data in Table 1 show, there was a considerable improvement in catalytic activity as the TiO_2 loading on the SiO_2 support was decreased.

A pair of representative HAADF and BF-STEM images (see the Experimental Section for technical details) acquired from the same region of Sample 1, which contained the greatest amount of TiO_2 and exhibited the lowest activity, are shown in Figure 1. HAADF imaging provides direct information of the

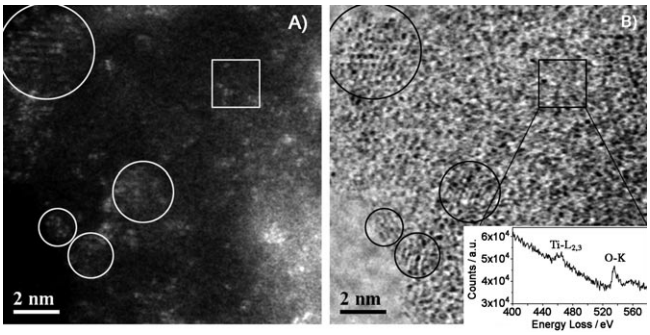

Figure 1. Representative pairs of A) HAADF and B) BF-STEM images from Sample 1, which contained the highest TiO_2 loading and exhibited the lowest activity; inset: a STEM-EELS spectrum collected from the area indicated by the square boxes in (A) and (B) showing weak Ti signals.

structure and distribution of the WO_x species by means of the atomic number (*Z*) contrast, whereas the phase contrast produced using BF-STEM imaging was used to locate the position and determine the structure/size of well-crystallized TiO_2 nanoparticles (as circled in the images). Individual W atoms are clearly resolved as bright spots in the HAADF image, which ensures that all the possible types of surface WO_x species are being imaged. Only part of the images are in focus in any one micrograph, owing to the reduced depth of focus in the aberration-corrected STEM instruments[22] and the intrinsic surface height variation of the catalyst. By comparing complementary

pairs of HAADF and BF-STEM images (Figure 1 and Figure S2), it is evident that most of the WO_x species tend to be atomically dispersed on the TiO_2 nanocrystals. However, a small fraction of the WO_x was found in regions where no distinguishable TiO_2 lattice fringes were observed in the corresponding BF-STEM images (as indicated by squares in Figure 1 and Figure S3). STEM-EELS was then applied to these areas to probe for the presence of any noncrystalline TiO_x species, which could not be easily detected in the BF images. Weak Ti signals were detected by scanning over the specimen regions, which exhibited WO_x species in the HAADF image; no Ti signals were detected in the regions devoid of WO_x species (Figure 1 and Figure S3). This suggests that these highly dispersed WO_x species are also associated with TiO_x entities (probably present as disordered polymeric TiO_x rafts), which do not give rise to lattice fringes by phase contrast due to a lack of periodic structure. The WO_x species are highly dispersed over the TiO_x rafts in the form of either isolated monotungstate or 2D polytungstate (i.e., $(WO_x)_n$ network structures with 2–6 W atoms linked by oxygen bridging bonds) species, as previously observed for the supported WO_3/ZrO_2 system.[19] No larger WO_x clusters/crystals, which would have been easily detected by using HAADF imaging, were found in this sample. It is also interesting to note that W atoms dispersed on crystalline TiO_2 domains have a strong tendency to locate themselves directly above the Ti atomic columns, as shown in Figure 1 A (and more clearly in Figure 4 C in which the TiO_2 nanocrystal is oriented along a major zone axis), which is a direct indication of strong bonding between the surface WO_x species and the underlying TiO_2 domains. These observations directly verify our previous conjecture, based on our previous Raman spectroscopy evidences, that the surface WO_x species possess a higher affinity for the TiO_x domains as compared with the SiO_2 support.[12]

A rather different structure and dispersion of WO_x was observed for Sample 2, which exhibited the highest catalytic activity and had the lowest TiO_2 loading. In a previous investigation of a similar catalyst using UV/Vis diffuse reflectance spectroscopy (DRS), it was proposed that the predominant TiO_x structure consisted of a polymeric species.[12] Although some individual W atoms (i.e., monotungstate and polytungstate species) could still be identified (Figure 2), a large number of WO_x clusters were present. The size distribution of the WO_x entities in this sample is shown in Figure 2 C. The dominant species were found to be clusters about 1 nm in size, containing (10–20) WO_x structural units. Analysis of BF-STEM and HRTEM imaging data
(Figure S4) did not reveal any lattice fringes from either TiO_2 or WO_3, confirming the absence of any well-crystallized structures in this sample. In an attempt to determine the composition of these disordered clusters, simultaneous STEM-EELS and STEM-XEDS spectra were acquired in a raster-scan mode (Figure 2 D). Weak but distinguishable Ti signals were detected in both EELS and XEDS spectra, whereas the W signal was only detected in the XEDS spectrum (owing primarily to the lack of any sharp EELS edge for W in the intermediate energy-loss region). These spectra suggest that the approximately 1 nm WO_x clusters are again associated with polymeric TiO_x entities. In contrast, STEM-EELS spectra taken from an area devoid of WO_x clusters (Figure S5) did not exhibit any Ti signal, indicating the incomplete coverage of the SiO_2 surface with TiO_x. Even though the equilibrium phase diagram of bulk TiO_2 and WO_3 does not suggest any solubility between these two components,[23] the possibility that the WO_x clusters observed in this sample may be intermixed with the amorphous TiO_x species cannot be ruled out, as the phase diagram may not be valid at the nanoscale and for surface phases.[24]

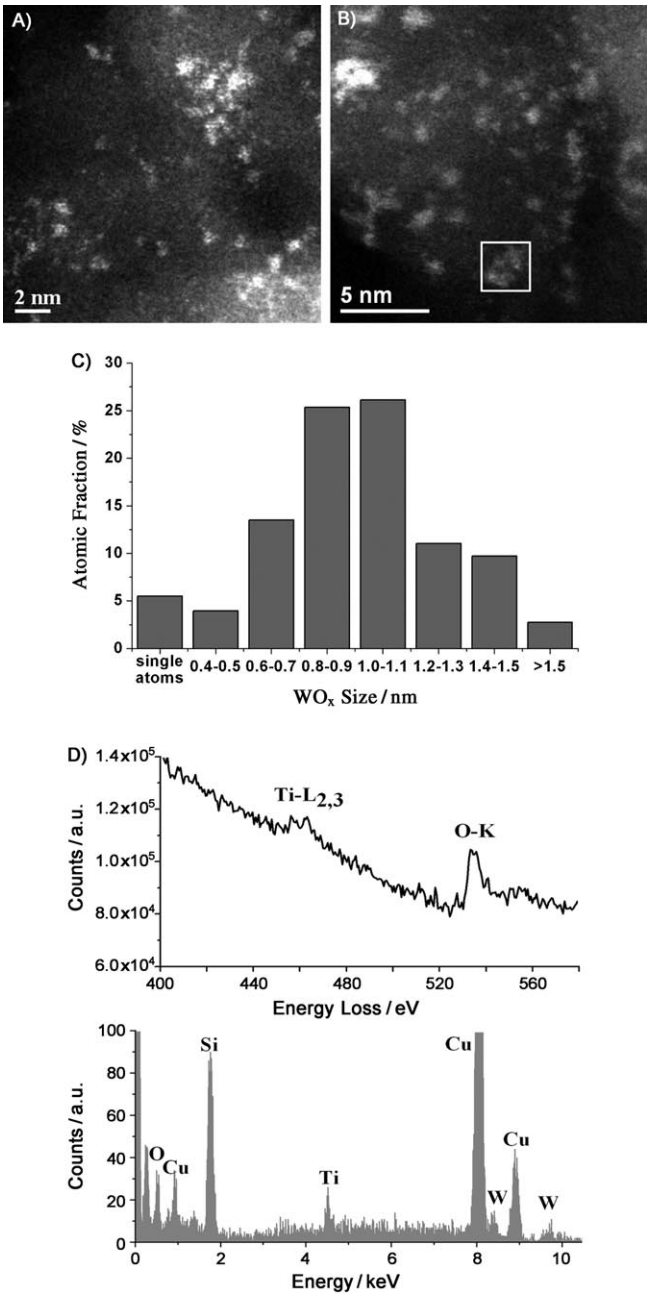

Figure 2. A, B) Representative HAADF images from Sample 2, which contained the lowest TiO_2 loading and exhibited the highest activity; C) size distribution of the WO_x entities in atomic fraction; D) STEM-EELS and XEDS spectra collected simultaneously from the $\approx$1 nm WO_x clusters indicated in (B). For the cluster size distribution, 250 clusters were measured from seven different images. The mean cluster size, excluding individual atoms, was 0.9 nm with a standard deviation of 0.3 nm.

EELS spectrum imaging[25,26] was applied to the highly-active Sample 2 to map out the distribution of Ti (as in TiO_x) and W (as in WO_x) on the SiO_2 surface. To reduce the electron-beam irradiation damage to the sample over the longer acquisition time required, the STEM accelerating voltage was reduced to 80 kV for this experiment, and a short dwell time was employed. Spatial-drift correction was applied during the data acquisition to compensate for any specimen drift, and multivariate statistical analysis (MSA)[27] was applied to the spectrum-image-data cube to improve the signal-to-noise ratio in the elemental maps. As shown in Figure 3 and Figure S6, the HAADF

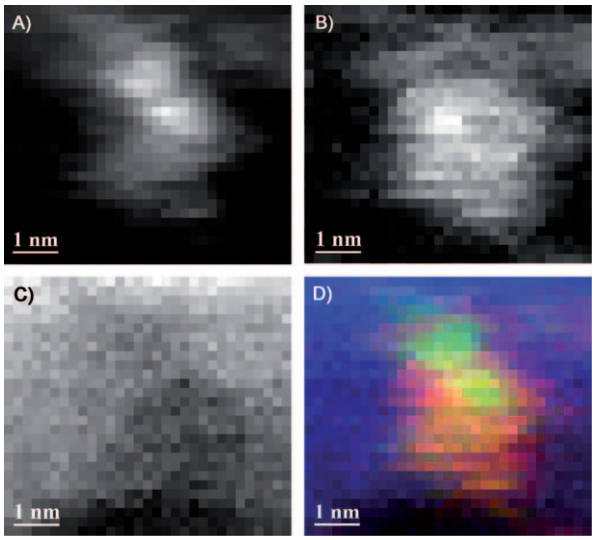

Figure 3. Simultaneous collection (at 80 kV from the highly active Sample 2—low TiO_2 loading) of A) HAADF image; B) STEM-EELS spectrum image using the Ti $L_{2,3}$ edge; C) STEM-EELS spectrum image using the oxygen K edge; D) the reconstructed map: HAADF signal in green, Ti $L_{2,3}$ EELS signal in red, and oxygen K edge EELS signal in blue.

signal, mainly contributed by the WO_x clusters, correlates well to the Ti $L_{2,3}$ edge EELS map, which confirms the close association of WO_x clusters with the TiO_x species. The oxygen K edge EELS map reveals the thickness variation of the SiO_2 support around the WO_x clusters. Even though the spectrum imaging was carefully performed, some structural modifications to this specific sample under the electron probe were still observed mainly due to the relatively weak bonding between the surface TiO_x rafts and the SiO_2 support.[28] However, the simultaneous collection of the HAADF and EELS signals ensures that the spatial correlation of WO_x and TiO_x is still valid, as the EELS signal originates from the same pixel as the HAADF signal.

For comparison, an intermediately active $WO_3/TiO_2/SiO_2$ catalyst (Sample 3) was also characterized by using STEM image analysis. As shown in Figure 4, most of the WO_x was atomically dispersed onto the surface of the TiO_x rafts as monotungstate and polytungstate (Figure 4 A), whereas some WO_x clusters (0.6–1.2 nm in size, circled in the images) were also found to nucleate on the noncrystalline TiO_x domains (Figure 4 B) and at the edges of some crystalline TiO_2 (anatase) nanoparticles that were sporadically found in this sample (Figures 4C,D). It is in-

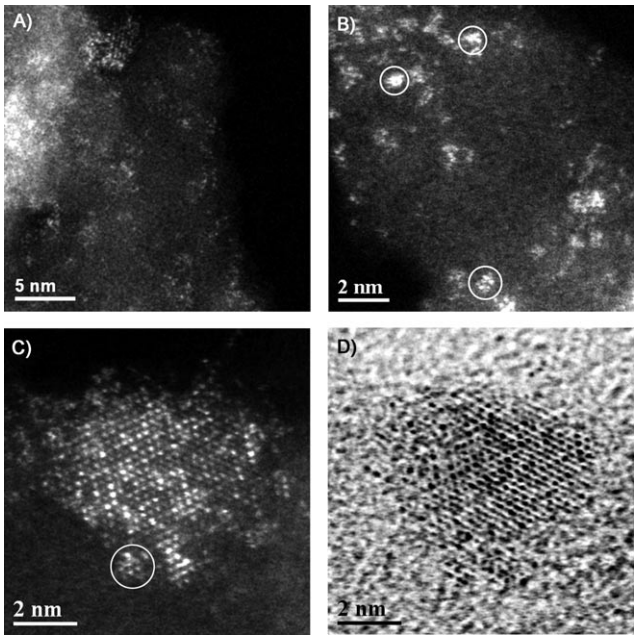

Figure 4. A–C) HAADF and D) BF-STEM images from Sample 3 (intermediate activity). The complementary pair of C) HAADF and D) BF-STEM images were taken from a TiO_2 (anatase-[201] projection) nanoparticle sporadically found in this sample.

teresting to note that the majority of the exposed surfaces of these "bulk" anatase particles were covered by mono- and polytungstate species (Figures 4A,C), suggesting that the WO_x clusters at the periphery were only formed after saturation of all the favorable surface TiO_x sites had taken place. A pair of HAADF and BF-STEM images shown in Figure 4C,D further illustrates the strong interaction between WO_x and the TiO_2 domains as evident by the fact that some Ti atomic columns in the HAADF image appear much brighter, owing to the additional presence of W atoms on these particular columns.

By comparing the structure of the double-supported WO_x catalysts discussed above with the structure of a model supported WO_3/SiO_2 material with similar WO_3 loading (Figure 5), it is clear that a preloaded TiO_x species on the SiO_2 surface can significantly alter the structure and dispersion of the WO_x load-

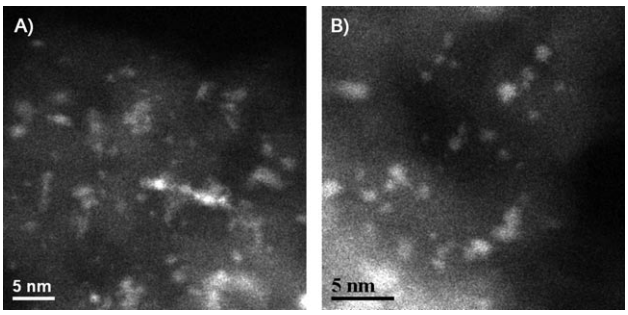

Figure 5. HAADF images taken from the model WO_3/SiO_2 material. This material was synthesized by means of an incipient-wetness impregnation procedure followed by high temperature calcination under air. The WO_x tends to form approximately 1 nm clusters on the amorphous SiO_2 surface. The WO_3 mass fraction in this sample was 5%.

ing. In particular, WO_x preferentially disperses on the TiO_x rafts, but can agglomerate into clusters after the saturation of available TiO_x surface sites in samples with lower TiO_2 raft density. In Sample 1 (low activity), the WO_x primarily presents as highly dispersed mono- and polytungstate species on larger TiO_2 domains. However, in Sample 2 (high activity), the approximately 1 nm WO_x clusters become the dominant structure. For the sample with intermediate catalytic activity (Sample 3), a mixture of both WO_x clusters and highly dispersed WO_x species were observed.

A study by Ross-Medgaarden et al.[12] revealed that the catalytic activities of these double supported WO_x catalysts, as determined from steady-state methanol dehydration reaction at 573 K, increased with a decreasing TiO_2 loading (Table 1). This activity trend was previously attributed to the gradually more localized electron density in the TiO_x nanoligand domains with decreasing TiO_2 loading, which then affects the charge-transfer behavior between the surface WO_x active species and the underlying TiO_x domains. Here we identify that there is an additional possible correlation between the increasing acidic activity of the double supported $WO_3/TiO_2/SiO_2$ catalysts and a structural change of the surface WO_x species. We also demonstrated that the 1 nm WO_x clusters supported on ZrO_2 possess higher acidic activity than the polytungstate and monotungstate species on the same support materials,[19] as a larger WO_x entity can more effectively disperse the extra electron density transferred from reactant molecules to the catalytic active sites during the reaction.[19,29] The presence of numerous the 1 nm WO_x clusters in the low TiO_2 loading sample, as opposed to the highly dispersed polytungstate and monotungstate species at high TiO_2 loading, could also contribute to the improvement in catalytic activity. Therefore, the catalytic activity in this double supported $WO_3/TiO_2/SiO_2$ catalyst system potentially displays a combined dependence on a) the different level of charge transfer between the supported WO_x species and underlying TiO_x domains and b) the change in physical and electronic structure of the surface WO_x species itself.

Conclusions

In summary, we have shown that the combined application of state-of-the-art aberration-corrected STEM imaging and chemical analysis techniques can overcome some of the difficulties associated with the structural characterization of complex double-supported metal oxide catalyst systems. Using complementary HAADF and BF-STEM imaging, together with STEM-EELS and XEDS chemical analysis, we have demonstrated that it is possible to map out the structure and relative distribution of all the metal oxide components in these double-supported $WO_3/TiO_2/SiO_2$ catalysts. In particular, for a constant level of WO_3 loading, the WO_x tends to be atomically dispersed on the larger TiO_x rafts, whereas the approximately 1 nm WO_x clusters are the preferred form on the smaller TiO_x domains. This atomic-scale structural information gives us new insight into the structure–performance relationships in this catalyst system. The catalytic acidic activity seems to benefit from a) a more localized electron density on the TiO_x support[12] and b) a large WO_x domain that can better disperse the electron density. We acknowledge that it is still an outstanding challenge to directly identify the structure of the polymeric TiO_x surface species in these double-supported catalyst samples using STEM imaging, which are known to be present from our complementary in situ Raman and UV/Vis spectroscopy studies of these samples.[12] Given the structural complexity associated with many specially designed, high-performance catalysts, we believe that this combined STEM imaging and chemical analysis approach, supplemented by invaluable in situ optical spectroscopy techniques, could play an important role in understanding the catalytic behavior of this general class of catalyst materials. Furthermore, with recent advances in electron microscope instrumentation, simultaneous HAADF imaging and ultra-fast STEM-EELS mapping at low kV[30] is now possible, which in principle opens new opportunities for the structural and chemical analysis of heterogeneous catalysts.

Experimental Section

The double-supported $WO_3/TiO_2/SiO_2$ catalysts were prepared by means of a two-step incipient-wetness impregnation procedure. Solutions of varying amounts of titanium isopropoxide [$Ti(OiPr)_4$] in isopropanol were impregnated onto pretreated amorphous SiO_2 supports, dried overnight under an N_2 flow in a glove-box, and subsequently calcined at 773 K under an air flow to form the TiO_2/SiO_2 support materials with different TiO_2 loadings. An aqueous solution containing a predetermined amount of ammonium metatungstate $(NH_4)_6H_2W_{12}O_{40}\cdot 5H_2O$ was impregnated onto the various TiO_2/SiO_2 materials and calcined at 723 K under an air flow to create the final double-supported catalysts with a constant WO_3 loading (5 wt%). A more detailed description of the synthesis method and catalyst testing procedures can be found in Reference [12].

Samples for electron microscopy analysis were prepared by dipping a carbon-coated copper TEM grid directly into the finely ground dry catalyst powder and then shaking off any loosely bound residue. Unless stated, the HAADF and BF-STEM images were taken by using a 200 kV JEOL JEM-2200FS (S)TEM equipped with a CEOS aberration corrector for illumination. Typically a coherent electron beam (FWHM $\approx$ 100 pm) with a probe current of approximately 30 pA was used for imaging, and dwell times between 48 μs and 60 μs per pixel were applied. Complementary pairs of HAADF and BF-STEM images were acquired in a sequential fashion because collecting these two signals simultaneously is not currently an option on our instrument. The focus setting was slightly adjusted between the HAADF images and BF-STEM images to compensate for the different optimum focus values in these two imaging modes. STEM-EELS and XEDS signals were acquired simultaneously using the same electron probe setting with the electron probe scanning continuously in a raster from a defined area. The STEM-EELS spectra were collected in a cumulative fashion for individual acquisition times of 1.2–2 s, and the total recording time was typically about 30–80 s depending on the signal intensity. The STEM-XEDS spectrum shown in Figure 2D was acquired for an additional 330 s (400 s in total) to obtain reasonable signals after the corresponding EELS spectrum was terminated.

Simultaneous HAADF and STEM-EELS spectrum imaging experiments were performed by using two aberration-corrected STEM instruments, both operating at 80 kV. Specifically, these were a JEOL JEM-ARM200F and a FEI Titan 80-300 (S)TEM. Typically, an electron

probe (with a current of approximately 100 pA) and 0.08–0.2 s per pixel dwell time were used for the acquisition. The spectrum imaging data acquired was processed with multivariate statistical analysis (MSA)[27] to enhance the signal-to-noise ratio in the elemental maps.

Acknowledgements

The authors gratefully acknowledge the financial support from the National Science Foundation's Nanoscale Interdisciplinary Research Team (NSF-NIRT) program under grant #0609018.

Keywords: catalysts · electron energy-loss spectroscopy · electron microscopy · high-resolution STEM imaging · Oxide

[1] J. M. Caruthers, J. A. Lauterbach, K. T. Thomson, V. Venkatasubramanian, C. M. Snively, A. Bhan, S. Katare, G. Oskarsdottir, *J. Catal.* **2003**, *216*, 98–109.
[2] K. L. Fujdala, T. D. Tilley, *J. Catal.* **2003**, *216*, 265–275.
[3] M. Tada, Y. Iwasawa, *J. Mol. Catal. A: Chem.* **2003**, *204*, 27–53.
[4] S. Saito, H. Yamamoto, *Acc. Chem. Res.* **2004**, *37*, 570–579.
[5] M. Tada, Y. Iwasawa, *Annu. Rev. Mater. Res.* **2005**, *35*, 397–426.
[6] G. J. Hutchings, *J. Mater. Chem.* **2009**, *19*, 1222–1235.
[7] J. K. Nørskov, T. Bligaard, J. Rossmeisl, C. H. Christensen, *Nat. Chem.* **2009**, *1*, 37–46.
[8] M. Neurock, *J. Catal.* **2003**, *216*, 73–88.
[9] M. Fernández-Garcia, A. Martinez-Arias, J. C. Hanson, J. A. Rodriguez, *Chem. Rev.* **2004**, *104*, 4063–4104.
[10] W. T. Wallace, B. K. Min, D. W. Goodman, *Top. Catal.* **2005**, *34*, 17–30.
[11] J. P. Gabaldon, M. Bore, A. K. Datye, *Top. Catal.* **2007**, *44*, 253–262.
[12] E. I. Ross-Medgaarden, I. E. Wachs, W. V. Knowles, A. Burrows, C. J. Kiely, M. S. Wong, *J. Am. Chem. Soc.* **2009**, *131*, 680–687.
[13] M. Varela, A. R. Lupini, K. van Benthem, A. Y. Borisevich, M. F. Chisholm, N. Shibata, E. Abe, S. J. Pennycook, *Annu. Rev. Mater. Res.* **2005**, *35*, 539–569.
[14] J. Y. Liu, *J. Electron Microsc.* **2005**, *54*, 251–278.
[15] S. Wang, A. Y. Borisevich, S. N. Rashkeev, M. V. Glazoff, K. Sohlberg, S. J. Pennycook, S. T. Pantelides, *Nat. Mater.* **2004**, *3*, 143–146.
[16] R. Erni, M. D. Rossell, C. Kisielowski, U. Dahmen, *Phys. Rev. Lett.* **2009**, *102*, 096101.
[17] K. Sohlberg, S. Rashkeev, A. Y. Borisevich, S. J. Pennycook, S. T. Pantelides, *ChemPhysChem* **2004**, *5*, 1893–1897.
[18] A. A. Herzing, C. J. Kiely, A. F. Carley, P. Landon, G. J. Hutchings, *Science* **2008**, *321*, 1331–1335.
[19] W. Zhou, E. I. Ross-Medgaarden, W. V. Knowles, M. S. Wong, I. E. Wachs, C. J. Kiely, *Nat. Chem.* **2009**, *1*, 722–728.
[20] A. Y. Borisevich, S. Wang, S. N. Rashkeev, M. Glazoff, S. J. Pennycook, S. T. Pantelides, *Adv. Mater.* **2007**, *19*, 2129–2133.
[21] D. B. Williams, C. B. Carter, *Transmission Electron Microscopy,* Plenum Press, New York, **1996**.
[22] A. Y. Borisevich, A. R. Lupini, S. J. Pennycook, *Proc. Natl. Acad. Sci. USA* **2006**, *103*, 3044–3048.
[23] L. L. Y. Chang, M. G. Scroger, B. Phillips, *J. Less-Common Met.* **1967**, *12*, 51–56.
[24] W. A. Jesser, G. J. Shiflet, G. L. Allen, J. L. Crawford, *Mater. Res. Innovations* **1999**, *2*, 211–216.
[25] C. Jeanguillaume, C. Colliex, *Ultramicroscopy* **1989**, *28*, 252–257.
[26] J. A. Hunt, D. B. Williams, *Ultramicroscopy* **1991**, *38*, 47–73.
[27] M. Watanabe, E. Okunishi, K. Ishizuka, *Microsc. Anal.* **2009**, *23* (7), 5–7.
[28] X. T. Gao, I. E. Wachs, *Catal. Today* **1999**, *51*, 233–254.
[29] D. G. Barton, M. Shtein, R. D. Wilson, S. L. Soled, E. Iglesia, *J. Phys. Chem. B* **1999**, *103*, 630–640.
[30] K. Suenaga, Y. Sato, Z. Liu, H. Kataura, T. Okazaki, K. Kimoto, H. Sawada, T. Sasaki, K. Omoto, T. Tomita, T. Kaneyama, Y. Kondo, *Nat. Chem.* **2009**, *1*, 415–418.

Received: August 4, 2010
Published online on November 29, 2010

